Modeling of Mach-Zehnder Interferometric Sensors Employing Ring-Resonator Circuits for Slow-Light Enhancement

Henri P. Uranus, *Senior Member, IEEE*

***Abstract*—The performance of symmetric Mach-Zehnder interferometric (*MZI*) sensor employing ring-resonator circuits for slow-light enhancement of the sensor performance was theoretically investigated. The slow-light structures considered in this study are coupled-resonator optical waveguide (*CROW*), four-port single ring-resonator (*FPRR*), and two-port single ring-resonator (*TPRR*) circuits. The performance of the sensors was quantitatively formulated for resolution of refractive index of measurand and figure of merit (*FoM*) with respect to similar *MZI* without employing slow-light structure. The effect of attenuation constant of mode traveling in the ring-resonator to the theoretical ultimate sensor resolution limited by available insertion loss budget was also discussed. Taking realistic ring attenuation constant of 1 dB/cm, ring radius of 300 μm, and 20 dB insertion loss budget, the theoretical ultimate sensing performance using a single-resonator *TPRR* can reach resolution of 3.63E-10 RIU which is 5 times better than single-resonator *FPRR* and 3-resonator *CROW* while giving *FoM* of 5 and 15 times better compared to circuit employing *FPRR* and 3-resonator *CROW*, respectively.**

***Index Terms*—Coupled-resonator optical waveguide, evanescent field sensor, Mach-Zehnder interferometer, refractive index sensor, ring-resonator, slow-light circuits.**

I. Introduction

IN SLOW-LIGHT [1] group velocity (v_g) of light is very slow with respect to its vacuum velocity (c), which imposes strong light-matter interaction that enhances processes in sensing [2], non-linear optics [3], light generation [4], light amplification [5], and energy harvesting [6]. Coupled-resonator optical waveguides (*CROW*s) [7], [8], [9] is one kind of structures which exhibit such slow-light phenomenon. Recently, a sensor utilizing a photonic crystal-based *CROW* has been demonstrated [10]. In simpler form, a *CROW* can also be constructed using coupled ring-resonators in the form of integrated optical waveguides [8], [9]. Hence, it is interesting to study integrated optical ring-resonator-based [11], [12] *CROW* for sensing applications, as it can be realized using simpler fabrication technologies than the photonic crystal counterpart.

Manuscript received 6 July 2023; revised 2 November 2023; accepted 5 November 2023. Date of publication 8 November 2023; date of current version 27 November 2023. This work was supported in part by the STW Technology Foundation under Grant TOE.6596 and in part by Universitas Pelita Harapan.

The author was with Integrated Optical MicroSystems Group, University of Twente, 7522 NB Enschede, The Netherlands. He is now with the Department Electrical Engineering, Universitas Pelita Harapan, Tangerang 15811, Indonesia (e-mail: henri.uranus@uph.edu).

Digital Object Identifier 10.1109/JPHOT.2023.3330985

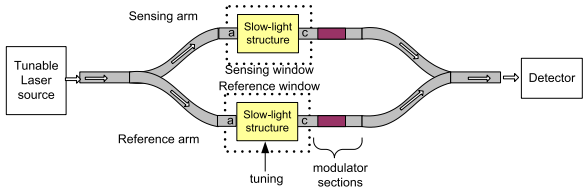

Fig. 1. Architecture of slow-light enhanced *MZI* sensor.

While a *CROW* has been considered as a slow-light structure, a single resonator circuit is also a potential slow-light structure [13], [14]. In fact, many attentions have been raised on enhancement of sensitivity of photonic sensors employing single ring resonator [15], [16], [17].

This paper reports theoretical study on the use of ring-resonator circuits as slow-light structures instead of ordinary waveguides in the arms of a symmetric refractometric *MZI* sensor [18] and study its performance enhancements. This paper is an extension of a preliminary conference report by the same author(s) appeared earlier [19]. Besides *CROW*, two kinds of single ring-resonator slow-light circuits were also considered. The sensors are evaluated in terms of measurand resolution, sensitivity, and figure of merit (*FoM*). It shows that the ring attenuation constant is important as it dictates the lower limit of the light group velocity and hence the ultimate resolution of the sensor. Using realistic values for the structure's parameters, it obtained that a theoretical refractive index resolution as low as around 2E-9 RIU is achievable using relative group velocity v_g/c of 1.05E-2 and 3.84E-3 in *CROW* consisting of 3 resonators and in four-port single ring-resonator (*FPRR*) circuit, respectively. However, using two-port single ring-resonator (*TPRR*) circuit, the theoretical resolution can even go down to 0.2 times with *FoM* of 5 times and 15 times better than *FPRR* and 3-ring *CROW*, respectively. The term *FPRR* refers to similar structure as *CROW* but with only single resonator, while *TPRR* refers to a straight waveguide with side-coupled single ring-resonator [13], [14].

II. Sensor Architecture and Performance Parameters

This work considers a symmetric *MZI* sensors with slow-light structures at both arms as shown in Fig. 1. At the sensing arm, there is a window where light propagating inside the resonator(s) interacts with the analytes in an evanescent sensing scheme.

© 2023 The Authors. This work is licensed under a Creative Commons Attribution-NonCommercial-NoDerivatives 4.0 License. For more information, see https://creativecommons.org/licenses/by-nc-nd/4.0/

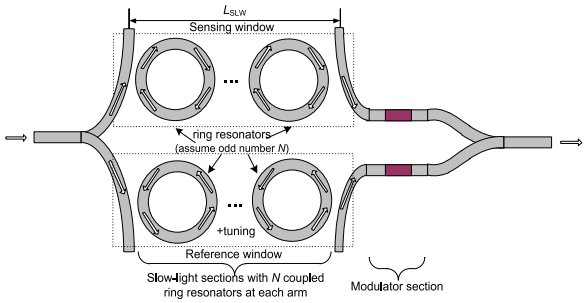

Fig. 2. Architecture of slow-light based *MZI* sensor employing *N*-ring *CROW* as the slow-light structure.

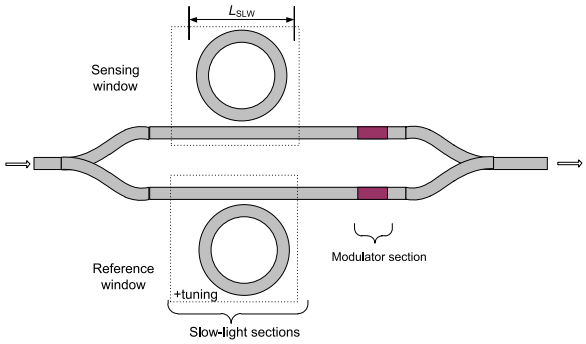

Fig. 3. Architecture of slow-light-based *MZI* sensor employing *TPRR* as the slow-light structure.

This analyte interrogation can either be a homogeneous sensing scheme or a surface sensing (through a bio- or chemo-receptor sensing layer) scheme. It is assumed that a tuning mechanism was employed in the reference arm in order to match both the level of signal and the resonant spectra of both arms. Hence changes in the analyte can be measured through the difference of phase of light passing the arms. It is assumed that the light source is tunable to the resonance wavelength of the slow-light structures. The *MZI* also assumed to incorporate serrodyne phase readout [18] scheme through e.g., modulators at both of its arms.

Employing *CROW* and *TPRR* circuits for the slow-light sections in the *MZI* leads to circuits shown in Figs. 2 and 3, respectively, while for *FPRR*, the circuit is just a reduction of Fig. 2 with number of resonator $N = 1$.

The group velocity of light passing a slow-light waveguide (*SLW*) is defined as

$$v_{\mathrm{g}} \equiv \frac{\partial \omega}{\partial \beta_{\mathrm{eff,SLW}}} = \frac{\partial \left(2\pi c/\lambda\right)}{\partial \beta_{\mathrm{eff,SLW}}} = -\frac{2\pi c}{\lambda^2} \frac{1}{\frac{\partial \beta_{\mathrm{eff,SLW}}}{\partial \lambda}} \tag{1}$$

where $\beta_{\mathrm{eff,SLW}}$, ω, λ, and c are the propagation constant in the *SLW*, the angular frequency, the vacuum wavelength, and the vacuum velocity of the light, respectively. Meanwhile, the group delay is defined by

$$\tau_{\mathrm{d}} \equiv \frac{\partial \phi}{\partial \omega} = \frac{L_{\mathrm{SLW}}}{v_{\mathrm{g}}} \tag{2}$$

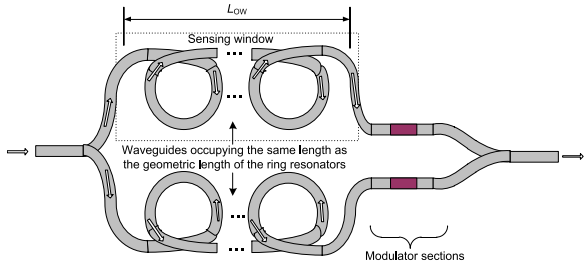

Fig. 4. Fictitious sensor layout used as a reference to define the figure of merit of the slow-light sensor being considered in this paper.

with ϕ and L_{SLW} denoting the phase changes after traveling across the *SLW* and the length of the *SLW* (as defined in the figures), respectively.

For interferometric refractive type ring-resonator sensor, the sensitivity of the sensor with respect to the measurand can be expressed as

$$S_{\mathrm{mea}} \equiv \frac{\partial \phi}{\partial n_{\mathrm{mea}}} = \frac{\partial \phi}{\partial n_{\mathrm{eff,res}}} \frac{\partial n_{\mathrm{eff,res}}}{\partial n_{\mathrm{mea}}} \tag{3}$$

where n_{mea} and $n_{\mathrm{eff,res}}$ denote the refractive index of the measurand and the effective index of the mode in the ring-resonator at the sensing arm, respectively. Using (2) and $n_{\mathrm{eff,res}} = \frac{\beta_{\mathrm{res}} c}{\omega}$ with β_{res} the propagation constant of mode in the ring-resonator, the first term in (3) becomes

$$\frac{\partial \phi}{\partial n_{\mathrm{eff,res}}} = \frac{\omega}{n_{\mathrm{eff,res}}} \tau_d = \frac{\omega L_{\mathrm{SLW}}}{n_{\mathrm{eff,res}} v_{\mathrm{g}}}. \tag{4}$$

Equation (4) shows the effect of slow-light to the sensitivity of the interferometer. Light with low v_{g} makes the interferometer to be more sensitive to the changes of the $n_{\mathrm{eff,res}}$. Note that the same sensitivity enhancement can be achieved by either decreasing the v_{g} or increasing the L_{SLW}. Hence, the slow-light phenomenon enables the enhancement of the sensitivity while keeping the device length short.

The refractive index resolution (δn_{mea}), i.e., the smallest refractive index changes resolvable by the sensor can be written as

$$\delta n_{\mathrm{mea}} = \frac{\delta \phi}{S_{\mathrm{mea}}} \tag{5}$$

where $\delta\phi$ denotes the phase resolution of the detection electronics.

In order to quantify the benefit of the slow-light sensor against similar sensor made of ordinary waveguide, this paper took a fictitious sensor layout as depicted in Fig. 4. It is assumed that this fictitious structure consists of ordinary waveguides at its arms, which have the same n_{eff} and geometric length as the sum of the circumference of the ring resonators in the slow-light sensor but without ring-resonator, hence assumed to occupy the same chip area as the slow-light sensor. The spiral tracks in Fig. 4 is just illustrative which can be considered similar to knot waveguides proposed by Brambilla [20] for optical fiber nanowire. *FoM* of the slow-light sensor is defined as the ratio between the sensitivity of the slow-light sensor against the

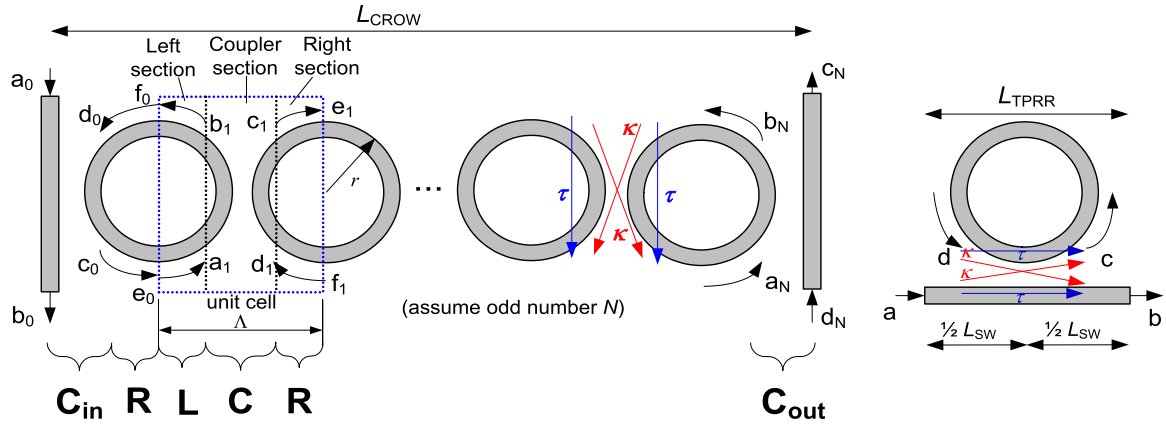

Fig. 5. (a) *CROW* and (b) the *TPRR* as the slow-light section and the notations used in the modeling. For *CROW*, the arrows in the figure denotes direction of light propagation for odd number of *N*.

fictitious ordinary-waveguide (*OW*) sensor as follows

$$FoM \equiv \frac{S_{\mathrm{SLW}}}{S_{\mathrm{OW}}} \approx \frac{\tau_{\mathrm{d,SLW}}}{\tau_{\mathrm{d,OW}}} = \frac{v_{\mathrm{g,OW}}}{\pi v_{\mathrm{g,SLW}}}. \tag{6}$$

Hence, the *FoM* can be regarded as the sensitivity gain of the slow-light sensor against the ordinary waveguide sensor of the same chip area occupation, or alternatively the chip area reduction (hence also the sensing analyte volume reduction) of the slow-light sensor against the ordinary waveguide sensor of the same sensitivity. Note that there are also different definitions of *FoM* in the literature.

Equations (3)–(6) reveal that slow-light enhances the sensor sensitivity and enables detection of smaller analyte changes within shorter device length, giving advantage measured in the *FoM* compared to an ordinary waveguide-based sensor of the same geometric length. Later in Section IV, it will be shown that there is limit in the slowness of the light, hence limit in the sensitivity and resolution enhancement in practice due to the fact that losses are unavoidable in the passive ring resonators and noises set the detection limit.

III. Modeling Ring-Resonator Circuits

In order to model the *CROW*, a transfer matrix method [21] was used to get the transmission coefficient of the structure. Expressing the transmission coefficient in complex quantity [22] enables the derivation of the group velocity. From there, other parameters related to the sensor performance were derived. This work assumes that both the ring resonator(s) and the access waveguides are single-mode. It is also assumed that the couplers are lossless and coupling only happens between adjacent waveguides. To be realistic, losses are considered in the ring-resonators.

The coupled rings in the *CROW* consist of unit cells which are subdivided into 3 sections as depicted in Fig. 5(a). For the coupling between two adjacent ring-resonators, the scattering matrix formulation is

$$\begin{bmatrix} b_{\mathrm{p}} \\ c_{\mathrm{p}} \end{bmatrix} = \mathbf{S} \begin{bmatrix} a_{\mathrm{p}} \\ d_{\mathrm{p}} \end{bmatrix} = \begin{bmatrix} \tau & \kappa \\ \kappa & \tau \end{bmatrix} \begin{bmatrix} a_{\mathrm{p}} \\ d_{\mathrm{p}} \end{bmatrix}$$

with τ and κ are the coupling constants, while a_{p} to f_{p} are the electromagnetic field's amplitude at particular positions in unit cell p as depicted in Fig. 5(a). Imposing unitary property ($\mathbf{SS}^{\mathrm{H}} = \mathbf{I}$) of the scattering matrix $\mathbf{S}$ into the formulation leads to following transfer matrix formulation

$$\begin{bmatrix} c_{\mathrm{p}} \\ d_{\mathrm{p}} \end{bmatrix} = \mathbf{C} \begin{bmatrix} a_{\mathrm{p}} \\ b_{\mathrm{p}} \end{bmatrix} = \begin{bmatrix} 1/\kappa^* & \tau/\kappa \\ \tau^*/\kappa^* & 1/\kappa \end{bmatrix} \begin{bmatrix} a_{\mathrm{p}} \\ b_{\mathrm{p}} \end{bmatrix}$$

where $\mathbf{C}$ is the transfer matrix of the coupler. The propagation in the left- and right-hand-side sections in the unit cell are expressed in

$$\begin{bmatrix} a_{\mathrm{p}} \\ b_{\mathrm{p}} \end{bmatrix} = \mathbf{L} \begin{bmatrix} e_{\mathrm{p-1}} \\ f_{\mathrm{p-1}} \end{bmatrix}$$

and

$$\begin{bmatrix} e_{\mathrm{p}} \\ f_{\mathrm{p}} \end{bmatrix} = \mathbf{R} \begin{bmatrix} c_{\mathrm{p}} \\ d_{\mathrm{p}} \end{bmatrix}$$

with $\mathbf{L}$ and $\mathbf{R}$ are the transfer matrices of corresponding left and right sections, which can be written as

$$\mathbf{L} = \mathbf{R} = \begin{bmatrix} \exp(-i\theta) & 0 \\ 0 & \exp(i\theta) \end{bmatrix} \tag{7}$$

where

$$\theta = (\beta_{\mathrm{res}} - i\alpha_{\mathrm{res}})\, \pi r/2 \tag{8}$$

is the phase-shift for propagation across a quarter ring, while r and α_{res} are the radius and the attenuation constant of the ring, respectively. Hence, for a single unit cell as depicted in Fig. 5(a), the formulation becomes

$$\begin{bmatrix} e_{\mathrm{p}} \\ f_{\mathrm{p}} \end{bmatrix} = \mathbf{RCL} \begin{bmatrix} e_{\mathrm{p-1}} \\ f_{\mathrm{p-1}} \end{bmatrix} = \begin{bmatrix} \exp(-2i\theta)/\kappa^* & \tau/\kappa \\ \tau^*/\kappa^* & \exp(2i\theta)/\kappa \end{bmatrix} \begin{bmatrix} e_{\mathrm{p-1}} \\ f_{\mathrm{p-1}} \end{bmatrix}$$
$$= \mathbf{M} \begin{bmatrix} e_{\mathrm{p-1}} \\ f_{\mathrm{p-1}} \end{bmatrix}$$

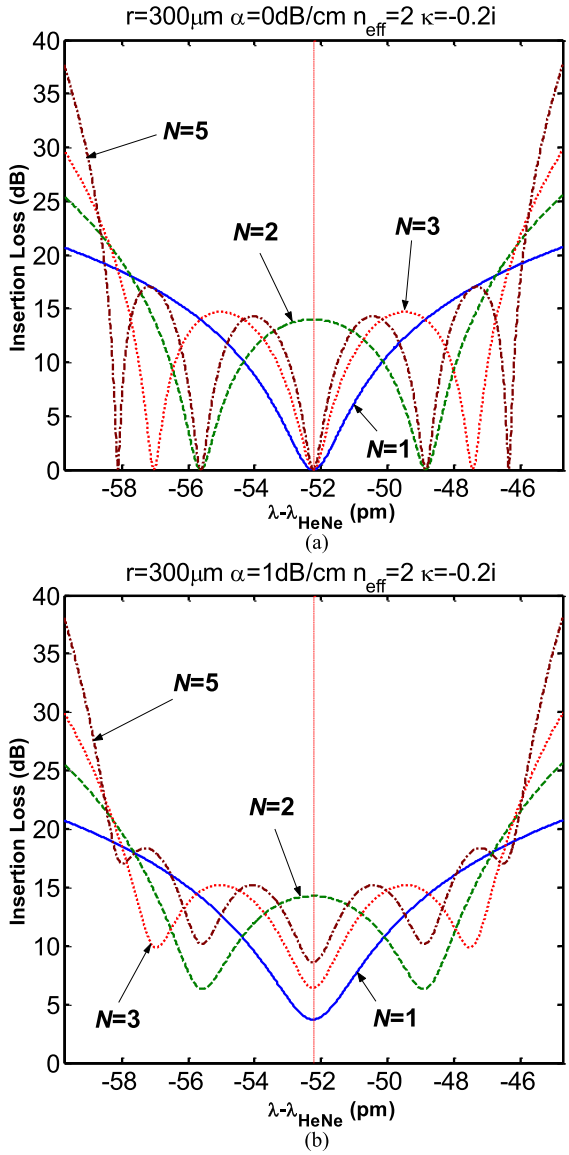

Fig. 6. Insertion loss of *CROWs* with various N and the *FPRR* with coupling constants of −0.2i for (a). Lossless ring(s), and (b). Lossy ring(s) with $\alpha_{\rm res} = 1$ dB/cm.

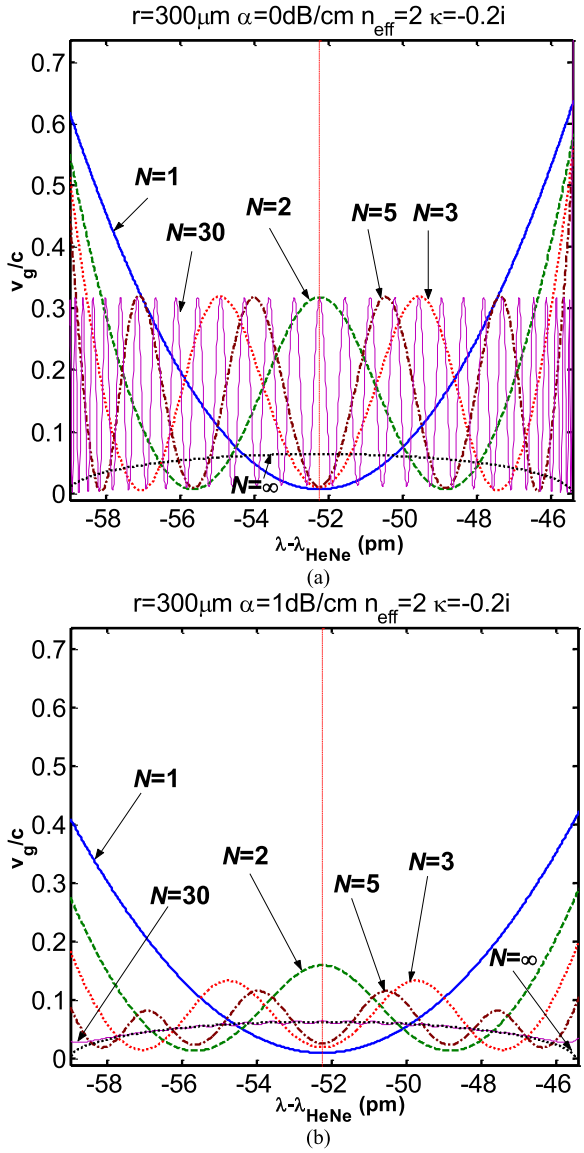

Fig. 7. Effect of number of coupled-resonators N of *CROW*s to the normalized group velocity for (a). Lossless ring(s), and (b). Lossy ring(s) with $\alpha_{\rm res} = 1$ dB/cm. Note: $N = 1$ denotes *FPRR*.

with $\mathbf{M} = \mathbf{RCL}$ is the transfer matrix of the unit cell. For a complete *CROW* structure with N coupled uniform resonators, successive multiplications of transfer matrices leads to

$$\begin{bmatrix} c_{\rm N} \\ d_{\rm N} \end{bmatrix} = \mathbf{C}_{\rm out}\mathbf{L}(\mathbf{RCL})^{N-1}\mathbf{RC}_{\rm in}\begin{bmatrix} a_0 \\ b_0 \end{bmatrix} = \mathbf{T}\begin{bmatrix} a_0 \\ b_0 \end{bmatrix} \tag{9}$$

where $\mathbf{C}_{\rm out}$, $\mathbf{C}_{\rm in}$, and $\mathbf{T}$ denote the transfer matrix of the output coupler, input coupler, and complete *CROW* structure respectively. For non-uniform resonators or couplers, (9) should be written in a long form

$$\begin{bmatrix} c_{\rm N} \\ d_{\rm N} \end{bmatrix} = \mathbf{C}_{\rm out}\mathbf{L}_{\rm N}\left(\mathbf{R}_{\rm N-1}\mathbf{C}_{\rm N-1}\mathbf{L}_{\rm N-1}\right)\ldots\left(\mathbf{R}_1\mathbf{C}_1\mathbf{L}_1\right)\mathbf{R}_0\mathbf{C}_{\rm in}\begin{bmatrix} a_0 \\ b_0 \end{bmatrix}$$

where each $\mathbf{R}_{\rm p}$, $\mathbf{C}_{\rm p}$, and $\mathbf{L}_{\rm p}$ represent the transfer matrices of corresponding section p of the structure. For $N = 1$, the structure reduces into *FPRR* circuit, which has transfer matrix formulation of

$$\begin{bmatrix} c_1 \\ d_1 \end{bmatrix} = \mathbf{C}_{\rm out}\mathbf{LRC}_{\rm in}\begin{bmatrix} a_0 \\ b_0 \end{bmatrix}.$$

By assuming that there is no back reflection from outside of the structure, the transmission coefficient can be written as

$$t_{\rm CROW} = \frac{c_{\rm N}}{a_0} = T_{11} - \frac{T_{12}T_{21}}{T_{22}} \tag{10}$$

where $T_{\rm mn}$ are elements of transfer matrix $\mathbf{T}$ at row m and column n. The transmission coefficient can also be expressed as

$$\begin{aligned} t_{\rm CROW} &= |t_{\rm CROW}|\exp\left(-i\phi\right) \\ &= |t_{\rm CROW}|\exp\left(-i\beta_{\rm eff,CROW}L_{\rm CROW}\right) \end{aligned} \tag{11}$$

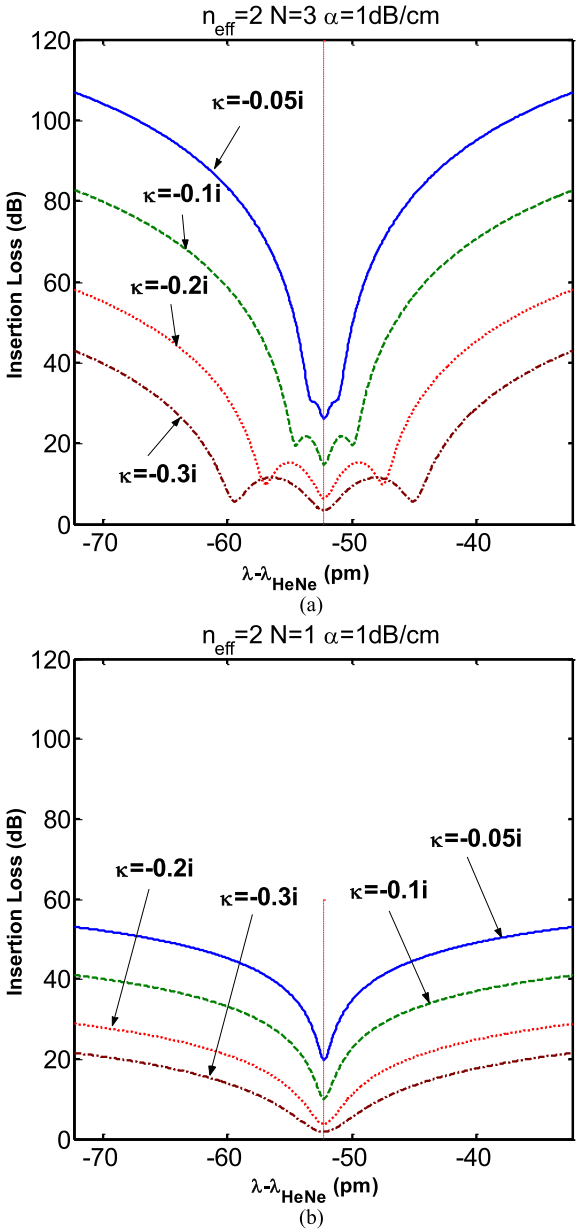

Fig. 8. Insertion loss of (a). a *CROW* with 3 resonators and (b). The *FPRR* for lossy ring(s) with $\alpha_{\rm res} = 1$ dB/cm for various values of coupling constant.

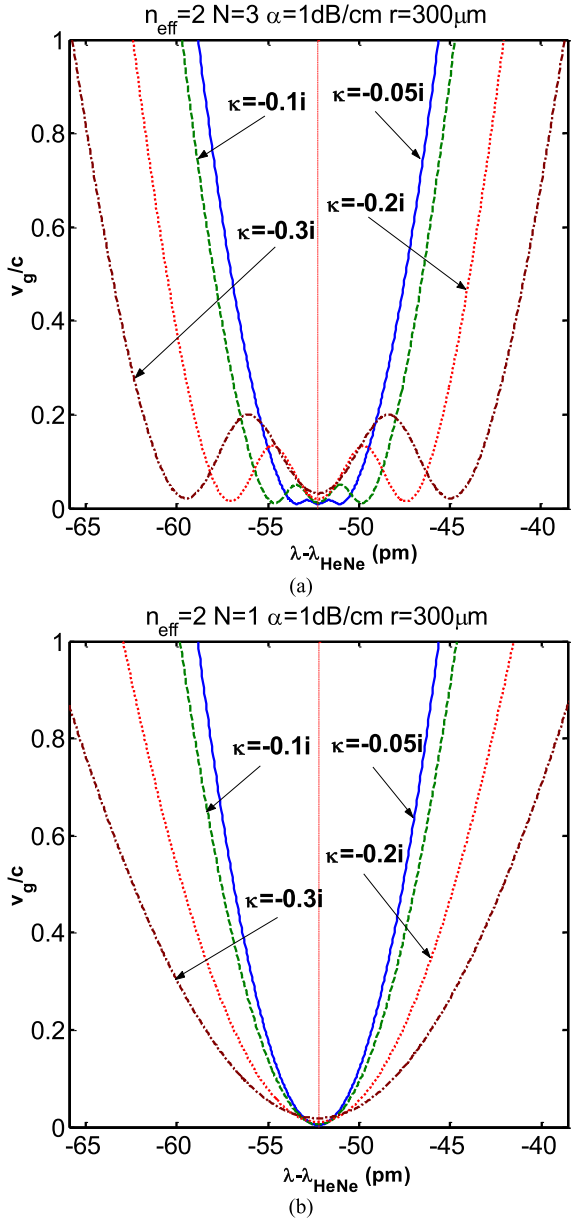

Fig. 9. Normalized group velocity of (a). A *CROW* with 3 resonators and (b). The *FPRR* of lossy ring(s) with $\alpha_{\rm res} = 1$ dB/cm for various values of coupling constant.

with

$$\phi = -\mathrm{Im}\left[\ln\left(t_{\rm CROW}\right)\right] \pm 2\pi q = \beta_{\rm eff,CROW} L_{\rm CROW} \qquad (12)$$

where q is an integer and Im[A] denotes the imaginary part of A, while $\beta_{\rm eff,CROW}$ and $L_{\rm CROW}$ are effective propagation constant and length of the *CROW*, respectively. By equating (10) and (11), values of parameters in (12) can be obtained and used to get sensor performance parameters in (1), (2), (3), (5), and (6) for *CROW*. Note that the measurand refractive index that affects the $n_{\rm eff,res}$ of mode in the rings, enters (10) through the phase change in (8).

Using similar method, following derivation in [13] the complex transmission coefficient of *TPRR* using notations in Fig. 5(b) can be written as

$$t_{\rm TPRR} \equiv \frac{b}{a} = \exp\left(-i\beta_{\rm SW} L_{\rm SW}\right) \frac{\tau + \exp\left(-i4\theta\right)}{1 - \tau \exp\left(-i4\theta\right)} \qquad (13)$$

where $\beta_{\rm SW}$ and $L_{\rm SW}$ are the propagation constant and length of the straight waveguide section, respectively, while θ is the phase shift in a quarter ring propagation as in (8). Using the complex transmission coefficient approach [22], results in

$$\begin{aligned} t_{\rm TPRR} &= |t_{\rm TPRR}| \exp\left(-i\phi_{\rm TPRR}\right) \\ &= |t_{\rm TPRR}| \exp\left(-i\beta_{\rm eff,TPRR} L_{\rm TPRR}\right) \end{aligned} \qquad (14)$$

with

$$\phi_{\rm TPRR} = -\mathrm{Im}\left[\ln\left(t_{\rm TPRR}\right)\right] \pm 2\pi m = \beta_{\rm eff,TPRR} L_{\rm TPRR} \qquad (15)$$

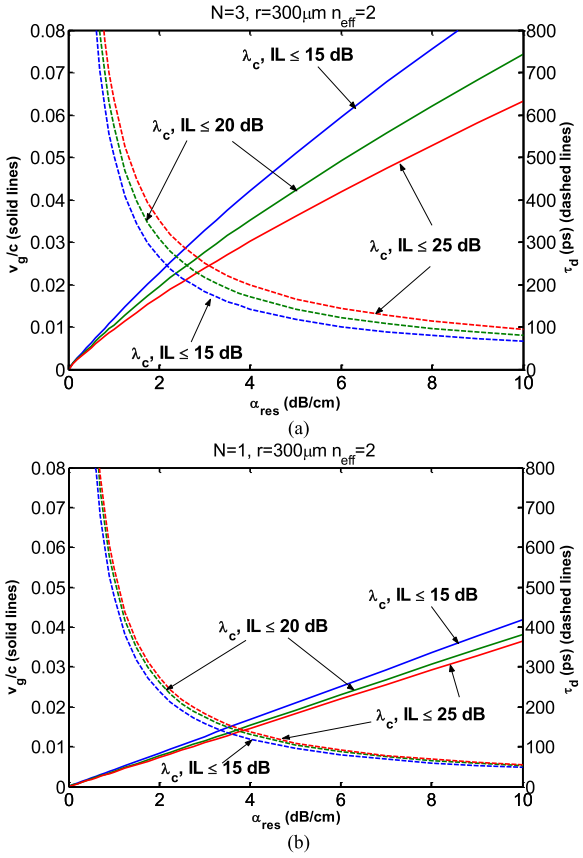

Fig. 10. Ultimate v_g/c and τ_d at the center resonant wavelength of (a). A 3-resonator *CROW* and (b). The *FPRR* as function of ring attenuation constant, under insertion loss budget of 15 dB, 20 dB, and 25 dB.

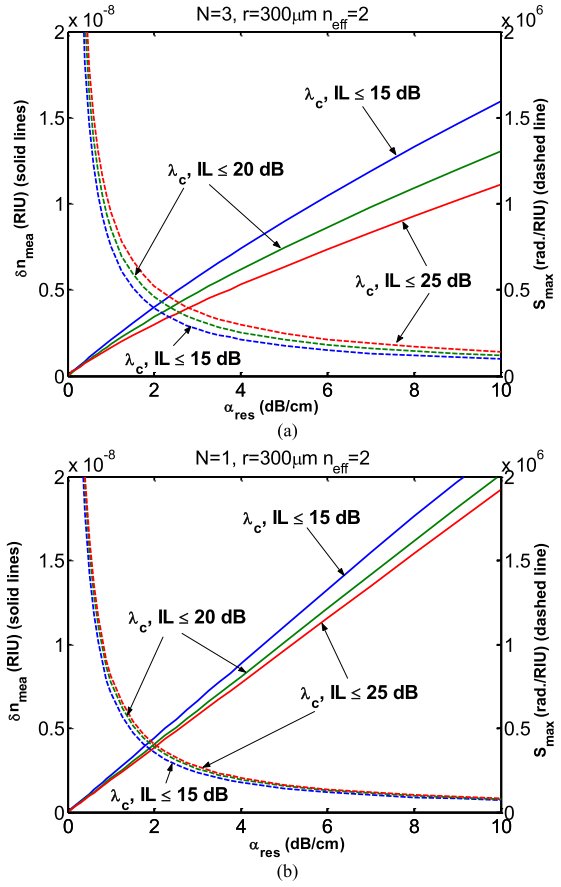

Fig. 11. Ultimate δn_{mea} and the sensitivity at the center resonant wavelength of (a). A 3-resonator *CROW* and (b). The *FPRR* as function of ring attenuation constant, under insertion loss budget of 15 dB, 20 dB, and 25 dB.

where m is an integer while $\beta_{\mathrm{eff,TPRR}}$ and L_{TPRR} are effective propagation constant and length of the *TPRR*, respectively. By equating (13) and (14), values of parameters in (15) can be obtained and used to get sensor performance parameters in (1), (2), (3), (5), and (6) for *TPRR*. Note that the measurand refractive index that affects $n_{\mathrm{eff,res}}$ of the mode in the rings, enters (13) through the phase change θ.

IV. Results and Discussions

As example, this work considers structures with slow-light section made of ring resonator(s) with radius $r = 300$ μm, effective index $n_{\mathrm{eff,res}} = 2$, working with resonance wavelength of the ring-resonator around 0.6328 μm (denoted as λ_{HeNe}). This is typical Si_3N_4-based ring-resonator similar to the one used in previous work [14]. Although the model discussed in this work is generally applicable, this particular structure was chosen simply due to the availability of its measured characteristics published in [14] in order to be realistic. The model presented in Section III was used to calculate the complex transmission coefficient around the resonant wavelength of the resonator(s) nearest to λ_{HeNe}, and then all other sensor's parameters given in Section II were calculated.

Firstly, the effect of the number of ring(s) (N) and the ring attenuation constant on the properties of the *CROW* consisting of uniform ring(s) was studied. The study was performed on various values of N, with ring attenuation constant of 0 dB/cm (lossless) and 1 dB/cm, and uniform coupling constant κ of -0.2i. Figs. 6 and 7 show the insertion loss and normalized group velocity of the light travels across the *CROW* structure. Note that $N = 1$ denotes *FPRR*. For the group velocity of the infinite structure, an eigenvalue equation as result of applying Bloch's boundary conditions to the unit cell was used. For the lossless-ring structure, the spectrum shows no insertion loss at the resonant wavelengths, at which the light gets slowed down. For single resonator structure, there is one resonant mode within one free spectral range, while for *CROW* with N resonators, the perturbation between resonant modes of N rings splits into N resonant modes, with the outermost resonant modes exhibit the lowest group velocity. Note that for a *CROW* with even N, there is no resonant mode coinciding with the resonant wavelength of an isolated single-ring with the same parameter, i.e., the wavelength denoted by the vertical line in the figures. However, since in reality the losses in passive resonators are unavoidable, then it is more realistic to consider the lossy *CROW*s. The figures show that for lossy *CROW*s, the slower the light, the higher the insertion loss of the resonant mode, as the light spends longer time inside the lossy resonator(s). Besides sensitivity, loss is also one of the products of light-matter interaction. So, the light slowness comes in the price of the insertion loss on one hand, but increases the light-matter interaction on the other hand. It is obvious that

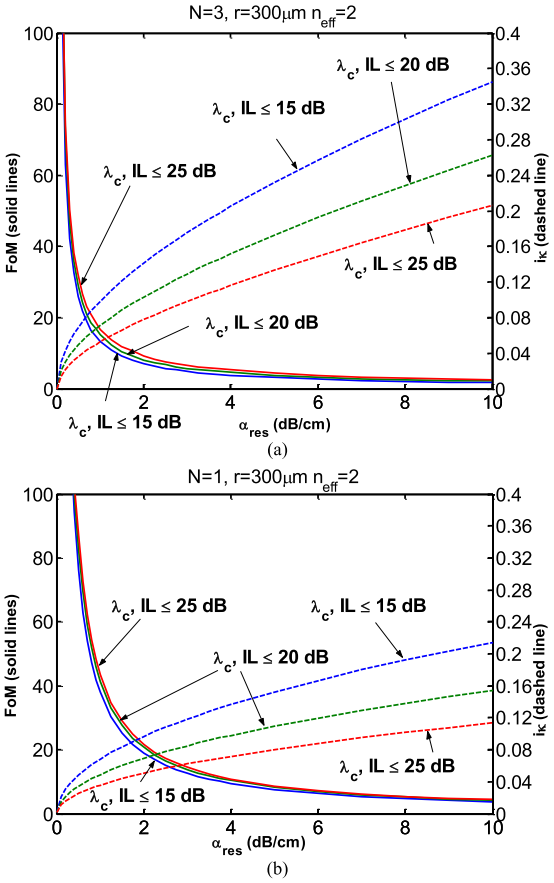

Fig. 12. Ultimate *FoM* and corresponding κ required to achieve such condition at the center resonant wavelength of (a). A 3-resonator *CROW* and (b). *FPRR* as function of ring attenuation constant, under insertion loss budget of 15 dB, 20 dB, and 25 dB.

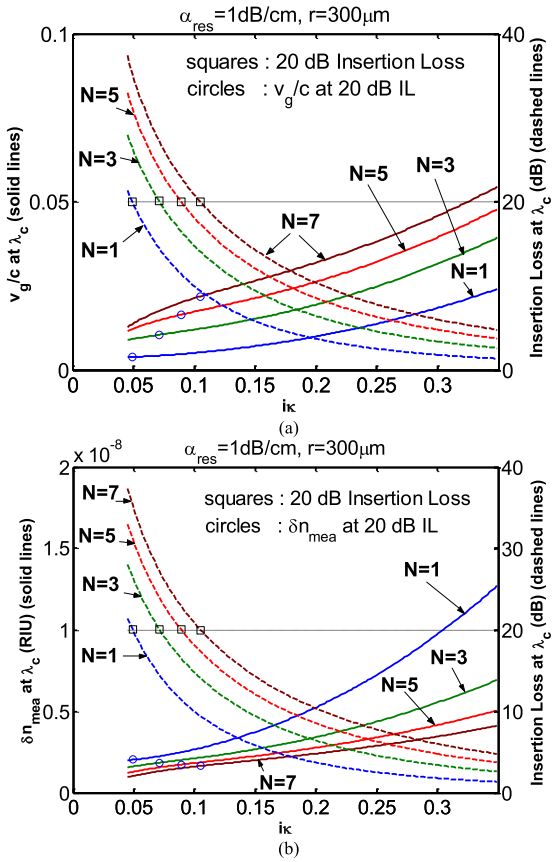

Fig. 13. (a) Normalized group velocity and insertion loss and (b). The resolution δn_{mea} and insertion loss of *CROW* with various values of N and the *FPRR* for 1 dB/cm ring attenuation constant. The squares and circles denote the points when insertion loss of 20 dB (the horizontal line) is achieved.

there is trade-off between light slowness and loss. In practice, there will be limit in the usable light slowness as dictated by the minimum detectable power of the detection electronics and the existence of noises. The losses make the resonant features to smear out, which at one hand increases the bandwidth, but at the other hand increases the insertion loss and v_{g} at wavelengths of interest, i.e., the resonant wavelengths where the local extrema of the slow-light phenomenon are located.

Since realizing *CROW* with large N requires high fabrication accuracy as non-uniformities can destroy the nice features of the *CROW*, this work will focus on *CROW* with small N. Besides, since resonator loss is unavoidable in practical passive *CROW*, the study will consider lossy structures of *CROW* with $N = 3$ and the single-resonator circuit with ring attenuation constant of 1 dB/cm, then explore the effect of the coupling constant. Figs. 8 and 9 show the insertion loss and the normalized group velocity of the lossy *CROW* and the single-resonator circuit for various values of the coupling constant. The smaller the coupling constant, the slower the light travels across the structure, as a smaller coupling constant makes the resonator to be more isolated. Similar to the previous results, the slower light comes in price of the higher insertion loss at the resonant wavelengths. The figures show that the single-resonator (i.e., *FPRR*) circuit can reach slow v_{g} which is comparable to the one produced by the *CROW*.

Taking into account that the allowable insertion loss is limited by the detector resolution, there is limit in the achievable light slowness in practice. Fig. 10 shows the lowest v_{g} and highest group delay at the center resonant mode as function of the ring attenuation constant, for a *CROW* with $N = 3$ and *FPRR* circuit. The results are limited by insertion loss budget of 15 dB, 20 dB, and 25 dB. Fig. 11 shows the minimum detectable measurand refractive index changes (i.e., the resolution) and maximum sensitivity under the same situation. Here homogeneous sensing scheme with $\partial n_{\mathrm{eff,res}}/\partial n_{\mathrm{mea}} = 0.2$ and resolution $\delta\phi = 5\mathrm{E}\text{-}5\times 2\pi$ rad. as given in [18] was used. This value of $\partial n_{\mathrm{eff,res}}/\partial n_{\mathrm{mea}}$ is typical value for refractometric homogeneous sensor using Si_3N_4 waveguide which already taken the field confinement and overlap with the analyte into account [18]. Fig. 12 shows the maximum *FoM* for the same situation. The situation for Figs. 10 to 11 is achieved using coupling constant as plotted at the right-hand axis of Fig. 12. Those figures show that both the *CROW* and the single-resonator *FPRR* circuit are slow-light structures, where frozen light (i.e., light with $v_{\mathrm{g}} = 0$) theoretically happens when the resonator is lossless ($\alpha_{\mathrm{res}} = 0$) and fully isolated from the outside world ($\kappa = 0$), which is unlikely to be used in reality. The higher sensor sensitivity can be achieved with smaller ring attenuation constant working in lower group velocity. Hence, research toward low loss ring resonator will be very important for such sensor applications. For the

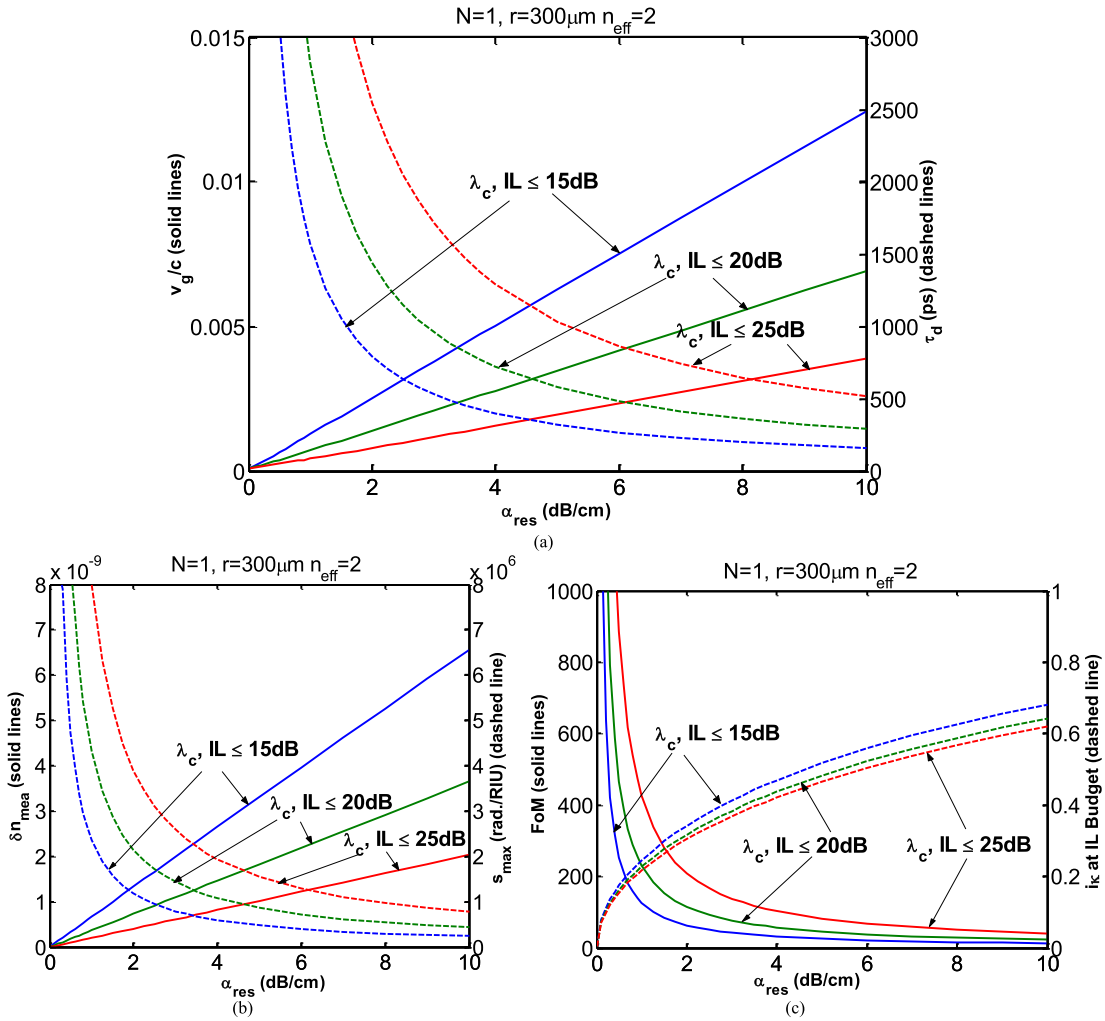

Fig. 14. (a) Ultimate v_g/c and corresponding τ_g, (b). $\delta n_{\rm mea}$ and sensitivity (c). *FoM* and κ required to achieve such condition at the center resonant wavelength of a *TPRR* circuit as function of ring attenuation constant, under insertion loss budget of 15 dB, 20 dB, and 25 dB.

same ring attenuation constant value and the same insertion loss budget, the light in an *FPRR* can stay longer in the resonator compared to the *CROW* structure. This means that a slower light can be achieved in an *FPRR* compared to the multiple-resonator *CROW*, but through a smaller coupling constant. Hence, the single-resonator circuit offers higher *FoM*. Moreover, in the regime of small attenuation constant, the sensitivity difference between *CROW* and *FPRR* becomes less significant. Being limited by insertion loss of 20 dB, using realistic ring(s) attenuation constant $\alpha_{\rm res} = 1$ dB/cm, both the 3-resonator *CROW* and the *FPRR* theoretically can achieve resolution $\delta n_{\rm mea}$ down to around 2E-9 RIU, using κ of around -0.07i and -0.05i which give v_g/c of around 0.01 and 0.004 for the *CROW* and the *FPRR*, respectively. The *FoM* for this situation are 15 and 41 for the *CROW* and the *FPRR*, respectively.

Fig. 13 shows the normalized group velocity and the resolution $\delta n_{\rm mea}$ along with the insertion loss of *CROW* with various values of *N* and the *FPRR* for 1 dB/cm ring attenuation constant. The squares and circles in the figures denote the points when insertion loss of 20 dB (the horizontal dotted line) is achieved. While smaller number of *N* needs to work with smaller coupling constant and slower light for the insertion loss limit of 20 dB, the *CROW* with larger number of *N* gains slightly better resolution due to its longer device length. However, this resolution improvement for larger *N* is not that significant for this particular low-value of ring attenuation constant regime. Since in practice large number of *N* will induce more fabrication complication, a single-resonator *FPRR* is more preferable for sensing applications. Besides, it is possible to achieve an almost similar resolution as the *CROW* counterpart for sufficiently small ring attenuation constant. The slow-light enhancement in the single-resonator sensor as reported in this paper also suggests that the sensing performance enhancement reported in the single ring-resonator sensing circuit reported by [15], [16], [17] are attributed to the slow-light phenomenon.

Using the same ring waveguide for *TPRR* results in Fig. 14 for normalized group velocity v_g/c and group delay τ_d, for resolution $\delta n_{\rm mea}$ and sensitivity $S_{\rm mea}$, and for *FoM* and coupling constant κ required to achieve ultimate condition under loss budget of 15 dB, 20 dB, and 25 dB. The results show that sensors with *TPRR* as the slow-light structure can theoretically achieve *FoM* of 231 and $\delta n_{\rm mea}$ of 3.6E-10 RIU with insertion loss budget

TABLE I
COMPARISON OF THE THEORETICAL ULTIMATE PERFORMANCE OF *CROW* WITH $N = 3$, *FPRR* AND *TPRR*, OBTAINED USING RING-RESONATOR(S) WITH $r = 300$ μm, $\alpha_{\rm res} = 1$ dB/CM, $n_{\rm eff} = 2$, AND LIMITED BY INSERTION LOSS BUDGET OF 20 dB

Parameters	3-resonator *CROW*	*FPRR*	*TPRR*
Min v_g/c	1.05E-2	3.84E-3	7.14E-4
Max n_g	95.5	260.7	1.4E3
Min δn_{mea}	1.84E-9 RIU	2E-9 RIU	3.63E-10 RIU
Max *FoM*	15.2	41.5	231
Max S_{mea}	8.5E5 rad/RIU	7.8E5 rad/RIU	4.3E6 rad/RIU
κ for the best performance	-0.07i	-0.0495i	-0.227i
Working at	Resonant peak nearest to λ_{HeNe}	Resonant peak nearest to λ_{HeNe}	Resonant dip nearest to λ_{HeNe}

of 20 dB on circuit with $\alpha_{\rm res} = 1$ dB/cm using κ of -0.227i and working with light as slow as $v_g/c = 7.1$E-4. This is more than 5 times and 15 times higher *FoM* than sensors with *FPRR* and 3-ring *CROW* made with same ring waveguide's parameters, respectively.

Table I summarizes the results and comparison between *MZI* sensors employing the three configurations of slow-light structures investigated in this work.

V. CONCLUSION

Refractive index sensors based on *MZI* enhanced with ring-resonator based slow-light structures for both of its arms were theoretically studied. The study includes *CROW* with $N = 3$, the *FPRR*, and the *TPRR*. The importance of ring(s) attenuation constant in limiting the usable slowness of light and the ultimate sensor resolution was revealed. For realistic attenuation constant, the performance of the *FPRR* is almost as good as the *CROW*. However, *TPRR* is shown to perform much better than the *FPRR* and *CROW*.

ACKNOWLEDGMENT

The author would like to thank Hugo J. W. M. Hoekstra for fruitful discussions.

REFERENCES

[1] J. B. Khurgin, "Slow light in various media: A tutorial," *Adv. Opt. Photon.*, vol. 2, no. 3, pp. 287–318, 2010.
[2] Z. Wu et al., "Investigation of a slow-light enhanced near-infrared absorption spectroscopic gas sensor, based on hollow-core photonic band-gap fiber," *Sensors*, vol. 18, no. 7, 2018, Art. no. 2192.
[3] N. Matsuda et al., "Slow light enhanced optical nonlinearity in a silicon photonic crystal coupled-resonator optical waveguide," *Opt. Exp.*, vol. 19, no. 21, pp. 19861–19874, 2011.
[4] W. Xue et al., "Threshold characteristics of slow-light photonic crystal lasers," *Phys. Rev. Lett.*, vol. 116, no. 6, 2016, Art. no. 063901.
[5] E. Shumakher, S. Ó. Dúill, and G. Eisenstein, "Optoelectronic oscillator tunable by an SOA based slow light element," *J. Lightw. Technol.*, vol. 27, no. 18, pp. 4063–4068, Sep. 2009.
[6] N. J. Thompson, D. N. Congreve, D. Goldberg, V. M. Menon, and M. A. Baldo, "Slow light enhanced singlet exciton fission solar cells with a 126% yield of electrons per photon," *Appl. Phys. Lett.*, vol. 103, no. 26, 2013, Art. no. 263302.
[7] A. Yariv, Y. Xu, R. K. Lee, and A. Scherer, "Coupled-resonator optical waveguide: A proposal and analysis," *Opt. Lett.*, vol. 24, no. 11, pp. 711–713, 1999.
[8] J. Scheuer, G. T. Paloczi, J. K. S. Poon, and A. Yariv, "Coupled resonator optical waveguides: Toward the slowing & storage of light," *Opt. Photon. News*, vol. 16, no. 2, pp. 36–40, 2005.
[9] A. Melloni, F. Morichetti, and M. Martinelli, "Linear and nonlinear pulse propagation in coupled resonator slow-wave optical structures," *Opt. Quantum Electron.*, vol. 35, pp. 365–379, 2003.
[10] H. Kurt and D. S. Citrin, "Coupled-resonator optical waveguides for biochemical sensing of nanoliter volume of analyte in the terahertz region," *Appl. Phys. Lett.*, vol. 87, 2005, Art. no. 241119.
[11] F. Michelotti, A. Driessen, and M. Bertolotti, "Microresonators as building blocks for VLSI photonics," in *Proc. Amer. Inst. Phys. Conf.*, 2004, pp. 1–18.
[12] C. K. Madsen and J. H. Zhao, *Optical Filter Design and Analysis: A Signal Processing Approach*. Hoboken, NJ, USA: Wiley, 1999.
[13] H. P. Uranus and H. J. W. M. Hoekstra, "Modeling of loss-induced superluminal and negative group velocity in two-port ring-resonator circuits," *J. Lightw. Technol.*, vol. 25, no. 9, pp. 2376–2384, Sep. 2007.
[14] H. P. Uranus, L. Zhuang, C. G. H. Roeloffzen, and H. J. W. M. Hoekstra, "Pulse advancement and delay in an integrated optical two-port ring-resonator circuit: Direct experimental observations," *Opt. Lett.*, vol. 32, no. 17, pp. 2620–2622, Sep. 2007.
[15] P. Lützow, D. Pergande, and H. Heidrich, "Integrated optical sensor platform for multiparameter bio-chemical analysis," *Opt. Exp.*, vol. 19, no. 14, pp. 13277–13284, 2011.
[16] J. T. Robinson, L. Chen, and M. Lipson, "On-chip gas detection in silicon optical microcavities," *Opt. Exp.*, vol. 16, no. 6, pp. 4296–4301, 2008.
[17] K. de Vos, I. Bartolozzi, E. Schacht, P. Bienstman, and R. Baets, "Silicon-on-insulator microring resonator for sensitive and label-free biosensing," *Opt. Exp.*, vol. 15, no. 12, pp. 7610–7615, 2007.
[18] R. G. Heideman and P. V. Lambeck, "Remote opto-chemical sensing with extreme sensitivity: Design, fabrication and performance of pigtailed integrated optical phase-modulated Mach-Zehnder interferometer system," *Sensors Actuators B*, vol. 61, pp. 100–127, 1999.
[19] H. P. Uranus and H. J. W. M. Hoekstra, "Enhancing the performance of integrated optical sensor by slow-light: Theoretical study on ring-resonator based structures," in *Proc. 2nd Int. Conf. Opt. Laser Appl.*, 2007, pp. 55–59.
[20] G. Brambilla, "Optical fibre nanotaper sensors," *Opt. Fiber Technol.*, vol. 16, no. 6, pp. 331–342, 2010.
[21] J. K. S. Poon, J. Scheuer, S. Mookherjea, G. T. Paloczi, Y. Huang, and A. Yariv, "Matrix analysis of microring coupled-resonator optical waveguides," *Opt. Exp.*, vol. 12, no. 1, pp. 90–103, 2004.
[22] J. M. Benedickson, J. P. Dowling, and M. Scalora, "Analytic expressions for the electromagnetic mode density in finite, one-dimensional, photonic band-gap structure," *Phys. Rev. E*, vol. 53, no. 4, pp. 4107–4121, 1996.